Journal of Medicinal Chemistry

Article

Pharmacophoric Features of Biguanide Derivatives: An Electronic and Structural Analysis

Prasad V. Bharatam, Dhilon S. Patel, and Pansy Iqbal

J. Med. Chem., **2005**, 48 (24), 7615-7622• DOI: 10.1021/jm050602z • Publication Date (Web): 03 November 2005

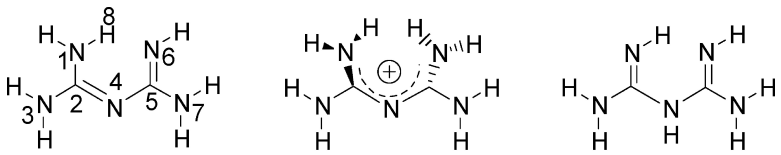

I II III

More About This Article

Additional resources and features associated with this article are available within the HTML version:

- Supporting Information
- Links to the 3 articles that cite this article, as of the time of this article download
- Access to high resolution figures
- Links to articles and content related to this article
- Copyright permission to reproduce figures and/or text from this article

View the Full Text HTML

Journal of Medicinal Chemistry is published by the American Chemical Society. 1155 Sixteenth Street N.W., Washington, DC 20036

Pharmacophoric Features of Biguanide Derivatives: An Electronic and Structural Analysis

Prasad V. Bharatam,* Dhilon S. Patel, and Pansy Iqbal

Department of Medicinal Chemistry, National Institute of Pharmaceutical Education and Research (NIPER), S.A.S. Nagar (Mohali) - 160 062, Punjab, India

Received June 24, 2005

The structure and electronic structure of drugs determine their mechanism of action. Correct structural representation of drugs helps in the proper identification of pharmacophoric features. Biguanide derivatives are a very important class of drugs, but their electronic structure was not clearly understood. Ab initio MO and density functional studies revealed the structure of the most stable tautomer of biguanide. (i) Electron delocalization, (ii) 1,3-H shift, (iii) 1,5-H shift, (iv) protonation, and (v) deprotonation processes, etc., have been investigated for biguanide. The molecular electrostatic potential (MESP) surfaces of neutral, protonated, and deprotonated biguanide have been shown to be similar in their most stable arrangements. The electrostatic potential of the complementary surface where these systems may bind also could be identified. Finally, the most stable structure of the important biguanide derivatives has been given after performing a conformational search.

Introduction

Biguanides are an important class of compounds that have extensive medical applications. Metformin[1] (**1**) (a blockbuster antidiabetic compound) and proguanil[2] (**2**) (an antimalarial agent) are biguanide derivatives, which are available as drugs. Other important compounds in this series are phenformin[3] (**3**), buformin[4] (**4**), chlorophenylbiguanide[5] (**5**), chlorhexidine[6] (**6**), etc. (Figure 1). Apart from the well-established antidiabetic and antimalarial effects, biguanide derivatives have been shown to exhibit antimicrobial,[6] antiviral,[7] antiplaque,[8] etc. effects and also have been known to influence gastric acid secretion.[9,10] The molecular mechanism of the therapeutic action of these systems is poorly understood. For example, the understanding about the molecular mechanism of metformin is still at a speculative stage. Holland et al. reported the tyrosine kinase stimulation by metformin.[11] More recently, evidence is being gathered to show the adenosine monophosphate kinase (AMPK) activation by metformin.[12−14] Sweeney et al. reported that phenformin and proguanil act as cysteine protease inhibitors, showing that the metal complexes of biguanide derivatives are more potent scaffolds for protease inhibitory activity.[15] Ruggiero-Lopez et al. and Mišur and Turk reported the advanced glycation end products (AGE) formation-inhibitory activity of biguanides.[16,17] Glennon et al. have reported 5-HT3 (Serotonin) receptor agonistic activity of arylbiguanide, and quantitative structure−activity relationship (QSAR) studies have been reported on this series.[5,18]

Biguanides are highly basic; they form HCl salts quite readily. This aspect is being exploited in the preparation of oral formulations of metformin.[19] Biguanides also are known to form dibasic salts such as biguanide·2HCl, biguanide·H_2SO_4, etc.[20] Biguanides also show acidic

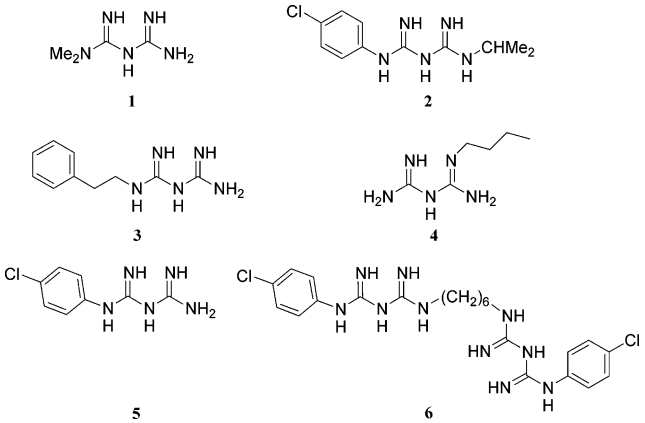

Figure 1. Various medicinally important biguanide compounds.

Scheme 1

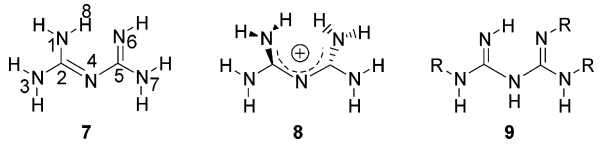

character. The anionic biguanides form complexes with transition metals.[21] Some of the metal complexes of biguanide include $[Mn(big)_3]^{4+}$, $B(big)_2Cl$, $[TcO(big)_2]^{3+}$, $[ReO(big)_2]^{3+}$, $Co(big)_3·2H_2O$, $[Cu(big)_2]^{2+}$, etc.[22−25] The crystal structures of neutral biguanide,[26] biguanide·HCl,[27] biguanide·2HCl,[28] and several metal complexes with biguanide derivatives are available.[21−25] The X-ray crystal structure of biguanide shows that structure **7** (Scheme 1) should be the most preferred structure,[26] without hydrogen on the bridging nitrogen (N4). The crystal structure of the HCl salt of biguanide (**8**) also does not show hydrogen on the bridging nitrogen (N4).[27]

However, in the medicinal chemistry literature, biguanide derivatives are always represented as structure

* To whom correspondence should be addressed. Phone: 91 172 221 4684. Fax: 91 172 223 3729. E-mail: pvbharatam@niper.ac.in..

10.1021/jm050602z CCC: $30.25
Published on Web 11/03/2005

9, which leads to a misleading perception. Especially when molecular modeling-based studies are being increasingly employed for the study of molecular mechanism, it is important to identify the appropriate structures and the detailed electronic charge distribution in biguanides.

The chemical, biochemical, and therapeutic activities of the biguanide derivatives and their variations can be attributed to the electron distribution in these systems. For example, the highly basic nature of biguanide derivatives is due to the increased electron delocalization upon protonation. Similarly, the complexation of the anionic biguanides with metals is due to the localization of charge density on the terminal nitrogens, which helps in the formation of chelating complexes. However, the electronic distribution in biguanides has not been studied in detail. In this paper, we report the electronic structure of the neutral, cationic, and anionic forms of biguanide. The protonation and deprotonation energies have been estimated using high-accuracy ab initio calculations. Natural bond orbital (NBO) analysis has been carried out to study the electron delocalization in various isomers of biguanide. We also report the tautomeric forms of biguanide, the most important 1,5-H and 1,3-H shift in biguanide.

Because the molecular recognition in drug−receptor interactions is driven by the stereo electronic effects of ligands, studies of three-dimensional MESP and its gradient plots have become important in characterizing pharmacologically active molecules.[29,30] As the drug action is a result of the complementarity of the electronic surface of the drug and the active site, it is important to understand the MESP of biguanides to comprehend the pharmacophoric features and their complementary surface. Thus, the comparative analysis of the MESPs of various isomers of biguanide provides clues regarding the complementary surface required for the binding of the biguanide-based drugs. In this paper, we include studies on the MESP surface of biguanide and its putative complementary surface.

Computational Details

Ab initio molecular orbital (MO)[31] and density functional (DFT)[32] calculations have been carried out using the GAUSSIAN03 software package.[33] Complete optimizations have been performed on various isomers of biguanide to understand the electronic structure, 1,3-H shift, 1,5-H shift, and C−N bond rotations using HF (Hartree−Fock), B3LYP (Becke3, Lee, Yang, Parr),[34] and MP2(full) (fully correlated Moeller−Plesset perturbation)[35] methods with the 6-31+G* basis set. Frequencies were computed analytically for all optimized species at all levels to characterize each stationary point as a minimum or a transition state and to estimate the zero point vibrational energies (ZPE). The calculated ZPE values (at 298.15 K) have been scaled by a factor of 0.9153, 0.9806, and 0.9661 for the HF, B3LYP, and MP2(full) levels, respectively.[36] The final absolute and relative energies were obtained using the high-accuracy Gaussian2-MP2 (G2MP2) method.[37] The protonated biguanides and deprotonated biguanides have been studied using the same method employed for biguanide. The NBO approach has been employed to quantitatively estimate the second-order interactions.[38] The harmonic oscillator measure of aromaticity (HOMA),[39] a geometry-based aromaticity index, has been applied to quantify the extent of π-electron delocalization of biguanide and related structures. Relative energies obtained using G2MP2[39] free energies and geometrical parameters observed in the MP2(full)/6-31+G*-optimized structure have been employed in the discussion unless otherwise specifically mentioned.

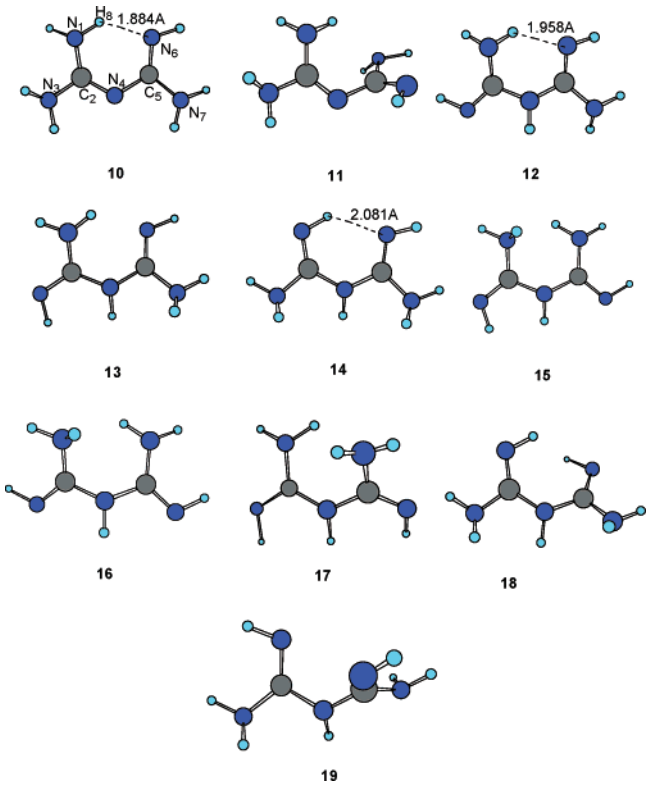

Figure 2. 3D structures of various tautomers of biguanide. Tautomers **10** and **11** do not have a hydrogen on N4, whereas tautomers **12**−**19** do have a hydrogen on N4.

The molecular electrostatic potentials were calculated on the MP2(full)-optimized geometries of selected biguanides and superimposed onto a constant electron density (0.002 e/au^3) to provide a measure of the electrostatic potential at roughly the van der Waals surface of the molecules using SPARTAN-*Pro* software.[40] The color-coded surface provides a location of the positive (deepest blue, most positive) and negative (deepest red, most negative) electrostatic potentials. The regions of positive charge indicate relative electron deficiency (estimated as a function of the repulsion experienced by a positively charged test probe), and regions of negative potential indicate areas of excess negative charge (estimated as a function of the attractive force experienced by a positively charged test probe).

Results and Discussion

Tautomers of Biguanide. Two different structural representations, **7** and **9** (Scheme 1), are in use for biguanide derivatives. Whereas representation **9** is generally employed in medicinal chemistry literature, representation **7** is chemically more accurate. Electronic structure studies showed that biguanide can exist in a total of 10 different tautomeric forms (Figure 2).[41] These tautomeric forms can be interconvertible using unimolecular 1,3-H shift processes or bimolecular paths involving protonated biguanide or anionic biguanide. The relative stabilities of these tautomers are given in Table 1. These 10 tautomers can be further subdivided in to two sets (i) those without hydrogen at the bridging nitrogen N4 (**10** and **11**) and (ii) those with hydrogen on the bridging nitrogen (**12**−**19**). Tautomers belonging to the first set (**10** and **11**) are relatively more stable compared to tautomers belonging to the second set (**12**−**19**). This clearly indicates that the presence of hydrogen on the central nitrogen is not a favorable process in

Table 1. Relative Energies (kcal/mol, ZPE corrected) of Various Conformers of **10** at 298.15 K Using 6-31+G* Basis Set

structure	HF	B3LYP	MP2	G2MP2[a]	chemical interpretation of the energy data[b]
10	0.00	0.00	0.00	0.00	Global Minimum
11	6.04	6.15	3.89	5.16	ΔE wrt **10**
12	7.55	7.62	7.39	5.66	-do-
13	10.20	9.90	9.21	7.78	-do-
14	11.26	11.76	9.67	9.34	-do-
15	11.74	11.49	9.97	9.53	-do-
16	12.65	12.45	11.16	10.07	-do-
17	12.66	12.20	11.18	10.21	-do-
18	13.05	13.43	11.35	10.97	-do-
19	18.67	19.01	16.86	16.17	-do-
20	10.85	3.87	5.24	4.18	1,5-H shift barrier in **10**
21	52.45	40.37	41.14	38.89	1,3-H shift barrier in **10**
22	11.18	11.41	10.66	10.47	Rot. Bar. across C2−N1 in **10**
23	13.93	12.40	12.48	11.09	Rot. Bar. across C2−N3 in **10**
24	13.94	13.09	13.08	12.39	Rot. Bar. across C5−N7 in **10**

[a] At the G2MP2 level, the relative energies are based on free energies. [b] ΔE is energy difference between tautomers, Rot. Bar. is the rotational barrier.

biguanides. Tautomers **10** and **11** are characterized by C2−N4−C5−N6(7) conjugation, which is absent in **12**−**19**. This basic conjugative interaction in **10** is further supported by delocalization from the lone pairs on amino nitrogens. The tautomers **12**−**19** are characterized by 6π-electron delocalization on the N=C2−N4−C5=N frame of these systems, where two electrons from N4 participate in π delocalization. Tautomer **10** is the most stable of all the tautomers, with all other tautomers at least >5 kcal/mol higher in energy (Table 1). The tautomeric representation generally given in medicinal chemistry literature is **14**; it is about 9.0 kcal/mol less stable than the most stable tautomer (**10**). This clearly indicates that the probability of the existence of tautomer **14** in equilibrium with **10** is almost negligible; according to Boltzmann formula, the concentration of tautomer **14** in a solution of biguanide turns out to be less than 0.001 ppm.

The three-dimensional (3D) structures of **10**, **12**, and **14** are given in Figure 2. **10** is characterized by a strong conjugation between C2−N4 and C5−N6 double bonds. It is also characterized by a strong intramolecular hydrogen bond, with a bond length of 1.884 Å at the MP2(full)/6-31+G* level. The combination of strong conjugation and intramolecular hydrogen bonding is responsible for the high relative stability of **10**. The N1−C2−N4−C5−N6 frame of **10** adopts an almost planar arrangement. **12** is also characterized by an intramolecular hydrogen bond (1.958 Å at the MP2 level). **14** is also characterized by intramolecular hydrogen bonding interaction; however, it is weaker than in **10** and **12** (2.081 Å at the MP2 level). **11** is 5.16 kcal/mol less stable than the global minimum **10**. In this tautomer, C2−N4−C5−N7 conjugation is expected, but steric repulsions due to N1 and N6 are very high and reduce the stability of this tautomer. Tautomer **13** is 7.78 kcal/mol higher in energy in relation to **10**; the absence of conjugative interaction is mainly responsible for the same. The other tautomers are higher-energy tautomers; the only surprising element is the identification of the high-energy local minimum **19** on the PE surface, which is not generally expected due to lone pair(N1)−lone pair(N6) repulsion.

To understand the energetics of the unimolecular H-transfer processes in biguanide, calculations have

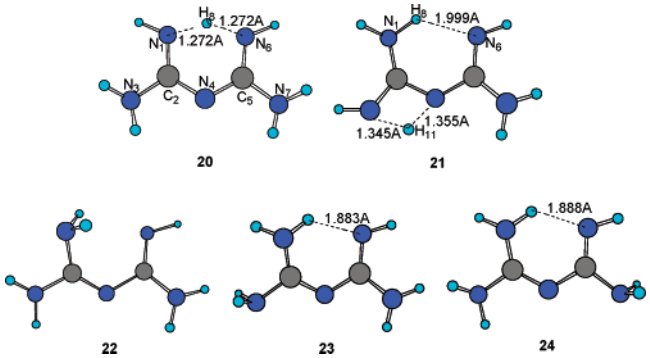

Figure 3. 1,5-H shift, 1,3-H shift, C2−N1, C2−N3, and C5−N7 rotational transition states of **10**.

Scheme 2

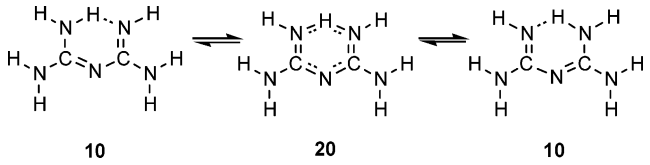

been performed to estimate the 1,5-H shift in **10** and the 1,3-H shift process between **10** and **12**. **10** may undergo a 1,5-H shift, between N1 and N6; this process does not lead to any new tautomer but may provide resonance stability to it. G2MP2 calculations showed that this process goes through a transition state (**20**) (Figure 3), with a barrier of about 4.18 kcal/mol; this small barrier indicates that there is a dynamical equilibrium between two resonating structures in **10** (Scheme 2). Such a 1,5-H shift is not practical in any other tautomer of biguanide (**12** or **14**) because it leads to the loss of conjugative stabilization. Hence, **10** gains additional stability due to resonance, as in Scheme 2. Transition state **20** is characterized by 6π-electron cyclic delocalization, which is responsible for the small energy barrier. The 1,3-H shift between tautomers **10** and **12** is represented by transition state **21** (Figure 3), with a H shift barrier of 38.89 kcal/mol at the G2MP2 level. This barrier is much less than the 1,3-H shift barrier estimated for acetaldehyde−vinyl alcohol (67.83 kcal/mol) and methylimine−vinylamine (65.49 kcal/mol) tautomeric processes at the same level.[42] However, the barrier is quite high, and the unimolecular path should not be expected in the tautomerism of biguanides.

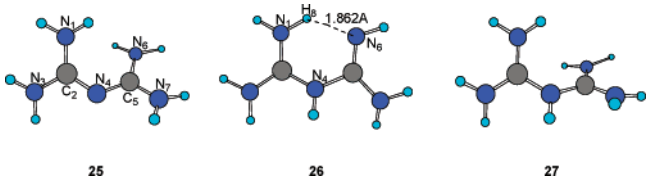

Figure 4. Protonated conformers of biguanide. **25** is N6-protonated, **26** is N4-protonated, and **27** is N4- and N6-diprotonated systems of **10**.

Electron Distribution in Biguanide 10. The extent of electron delocalization can be estimated in terms of (i) C−N rotations in biguanide, (ii) NBO analysis, and (iii) HOMA analysis.[42,43] The C2−N1, C2−N3, and C5−N7 bonds are expected to be single bonds with partial π character. The rotational barriers across these bonds respectively are 10.47, 11.09, and 12.39 kcal/mol through the rotational transition states **22**, **23**, **24** (Figure 3). These values are slightly larger than the C−N rotational barriers in guanidine (10.84 kcal/mol);[42a] all values are at the G2MP2 level, suggesting that the extent of π delocalization is slightly greater in biguanide compared to that in guanidine.

Natural bond orbital (NBO) analysis provides information regarding the electron delocalization from any lone pair. In **10**, the occupancy of N1, N3, and N7 lone pairs are 1.80, 1.87, and 1.87, respectively, indicating greater delocalization from N1. The energy $E^{(2)}$ associated with the second-order delocalization $n_{N1} \rightarrow \pi^*_{C2-N4}$ is 83.38 kcal/mol. The $E^{(2)}$ associated with $n_{N3} \rightarrow \pi^*_{C2-N4}$ and $n_{N7} \rightarrow \pi^*_{C5-N7}$ are 51.28 and 50.36 kcal/mol, respectively. All of these second-order interactions are larger than the $n_N \rightarrow \pi^*_{C-N}$ delocalization observed in guanidine ($E^{(2)} = 46.09$ kcal/mol),[42a] demonstrating that stabilization due to electron delocalization in biguanide is very high. A quantitative measure of the extent of delocalization can be calculated using the geometry-based aromaticity index HOMA. The HOMA parameter for **10** is 0.819, larger than the same for **13** (0.741) and **15** (0.615), indicating that the electron delocalization in **10** is greater.

Protonation in Biguanide 10. The partial atomic charges obtained from natural population analysis (NPA)[38] showed that a large negative charge is present on N4 (−0.79) and on N6 (−0.95) in **10** (Table S4), which indicates that the most favored protonation site in biguanide is N6. The highest occupied molecular orbital (HOMO) of **10** is mainly based on the N6 lone pair, supporting the conclusion that protonation is favorable at the N6 site. Maksik et al. reported that N6 is the favored protonation site on the basis of protonation energies.[44] The MESP data also supports that N6 is the preferred site for protonation in **10**. The crystal structure report on protonated biguanide also supports the N6-protonated structure.[27] Mono protonation on **10** at N6 gives **25**, and protonation at N4 gives **26**; these two structures are tautomers. **25** is a C_2 symmetric system (Figure 4) with a 22.4° torsional angle across C2−N4−C5−N6 at the MP2(full)/6-31+G* level, which is comparable to the X-ray report (22.7°).[27] **26** possesses an intramolecular hydrogen bond, with a bond length of 1.862 Å; it has an almost planar structure. The double-protonated biguanide **27** is also a C_2 symmetric system with a 31.1° torsional angle across C2−N4−C5−N6.

Table 2. Protonation Energies of 10 (in kcal/mol)

product of protonation	HF/ 6-31+G*	B3LYP/ 6-31+G*	MP2(full)/ 6-31+G*	G2MP2
25	−247.71	−241.63	−237.28	−250.53
26	−234.72	−230.47	−227.40	−241.51
28	−365.56	−356.94	−351.04	−367.44

Scheme 3

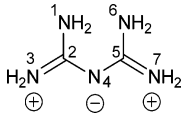

25 is more stable than **26** by ∼9.0 kcal/mol at the G2MP2 level (Table 2). This greater preference for N6 protonation is surprising because it causes breaking of the intramolecular hydrogen bond and also reduces C2−N4−C5−N6 conjugation. However, there is a possibility of increased resonance stabilization, as pointed out by Maksik et al.[44] The Gibbs free energy for protonation at N6 and N4 in **10** is −250.53 and −241.51 kcal/mol at the G2MP2 level, respectively.[45] In comparison to the Gibbs free energy for protonation in guanidine (−229.42 kcal/mol at the G2MP2 level),[42] the protonation is a much more favorable process in biguanide—on a relative scale, protonation at N4 is less stabilizing and protonation at N6 is more stabilizing in **10**. The HOMA values for **25** (0.985), **26** (0.794), and **27** (0.892) clearly indicate the greater electron delocalization in **25** (Table S7). The greater electron delocalization induced is responsible for the greater stabilization of **25** relative to that of **26**. NBO analysis showed that N4 in **25** contains two lone pairs and that there are two double bonds, C2−N3 and C5−N7. There are two strong second-order interactions $n_{N4} \rightarrow \pi^*_{C2-N3}$ and $n_{N4} \rightarrow \pi^*_{C5-N7}$, both with very high $E^{(2)}$ values of 139.6 kcal/mol. NBO analysis indicates that **25** should be treated as a 6π-electron conjugated system N1−C2−N4−C5−N7, which also gets stabilized by electron delocalization from N1 and N6 lone pairs (Scheme 3). This is also supported by the geometric parameters C2−N3, C2−N4, C5−N4, C5−N7 bond lengths that are in the range of 1.333−1.336 Å, whereas C2−N1 and C5−N6 bond lengths are in the range of 1.356 Å in **25**.

Deprotonation in Biguanide 10. As discussed in the Introduction, several complexes of deprotonated biguanide with transition metal systems have been reported. Besides, the bimolecular tautomerisation in neutral biguanide might be taking place via an anionic species (**28**−**30**). For example, the tautomeric proton exchange between **10** and **12** might involve **30** (Figure 5). In principle, any of the hydrogen atoms (H8−H14) can be involved in deprotonation. The synthesized metal complexes indicate that the deprotonation of H8 is the most prominent. However, H8-deprotonated biguanide become highly unstable in the absence of metallic complexation; this is because of the repulsions between lone pairs of electrons N1 and N6 in such a state. The deprotonation of H12−H14 is also not favorable due to a decrease in resonance destabilization. Hence, deprotonation of H9−H11 has been considered in this study. The Gibbs free energies due to deprotonation of H9−H11 in **10** respectively are 345.44, 344.32, and 349.40 kcal/mol at the G2MP2 level (Table 3). These ionization energies are less than those of acetaldehyde (366.74),

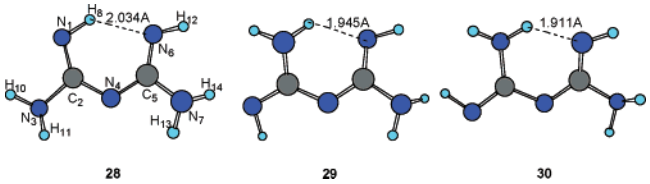

Figure 5. Deprotonated forms of biguanide **10**. **28** is H9-deprotonated, **29** is H10-deprotonated, and **30** is H11-deprotonated tautomers of anionic biguanide.

Table 3. Deprotonation Energies of 10 (in kcal/mol)

product after deprotonation	HF/ 6-31+G*	B3LYP/ 6-31+G*	MP2(full)/ 6-31+G*	G2MP2
28	361.33	354.71	350.00	345.44
29	360.07	352.70	348.88	344.32
30	366.87	358.47	355.13	349.40

acetaldimine (377.03), or nitromethane (358.17 kcal/mol), which are known to be involved in keto−enol, imine−enamine, and nitro−*aci*nitro tautomeric processes. Hence, it may be inferred that biomolecular tautomerization involving the deprotonation pathway in biguanide should be more favorable than the same process in keto−enol, imine−enamine and nitro−*aci*nitro tautomeric processes. This relatively high acidity of biguanides is responsible for the ready formation of metallic complexes and probably plays an important role in the biological processes. **29** represents the structure of the lowest-energy anionic biguanide. This species is characterized by two lone pairs on N4, according to NBO analysis. The geometric parameters of **29** as well as the electronic structure based on NBO analysis show the presence of a clear C2−N3 double bond. The $n_{N4} \rightarrow \pi^*_{C2-N3}$ and $n_{N4} \rightarrow \pi^*_{C5-N6}$ energy $E^{(2)}$ with the second-order interaction in **29** is 67.2 and 105.97 kcal/mol, respectively, indicating the greater delocalization of electron density.

Scheme 4

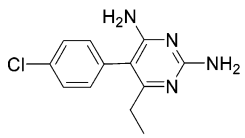

31

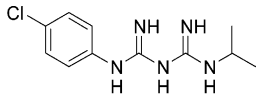

2

Scheme 5

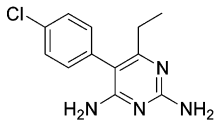

32

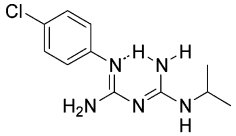

33

Molecular Electrostatic Potential Analysis. Figure 6 shows the molecular electrostatic potentials (MESP) of **10**, **12**, **14**, **25**, and **29**. The electrostatic potential of **10** shows the concentration of electron density at N4. Clearly, there is a large difference in the MESP of **14** with respect to that of **10**. Hence, the representation of biguanides and their derivatives as **14** only lead to misleading expectations about the complementary surfaces on the biomolecules. Because **10** is the most stable arrangement, a complementary surface for the same should be similar to that in Figure 6d; such an understanding of the electrostatic complementarity is particularly important in the wake of current work on molecular docking of biguanide derivatives in active sites of the cystine protease enzyme,[14] etc. The molecular electrostatic potentials of **25** and **29** also are quite similar to that of **10**, especially in the

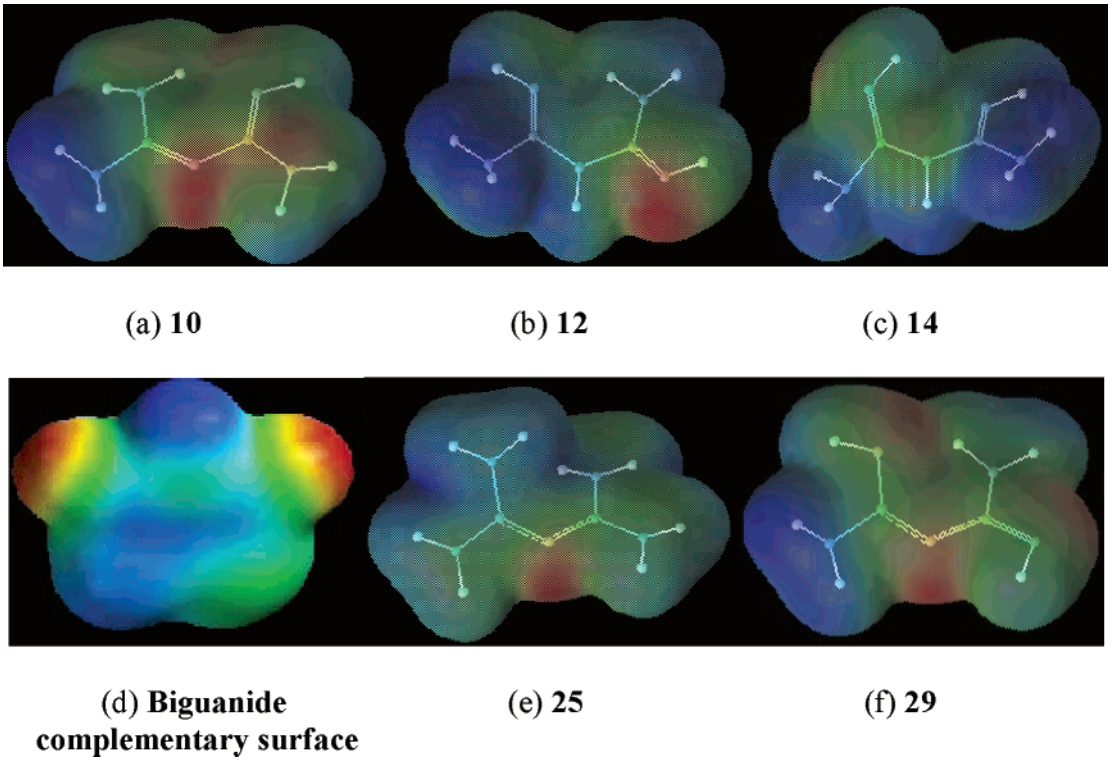

Figure 6. Molecular electrostatic potential (MESP) surfaces of selected biguanides and proposed complementary surface for biguanides plotted onto a surface of constant electron density (0.002 e/au^3) showing the most positive potential (deepest blue color), the most negative potential (deepest red color), and the intermediate potential regions (intermediate shades).

C3−N4−C5 region. Hence, the complementary surface for the biguanides may not be quite different when the biguanides exist in their cationic/anionic states.

Pharmacophoric Features and Electronic Structure. In the introduction, it was shown that structure **9** in Scheme 1 is most often employed in medicinal chemistry literature for biguanides. Such a representation masks the pharmacophoric features of biguanide derivatives. For example, pyrimethamine (**31**) and proguanil (**2**) are dihydrofolate reductase (DHFR) inhibitors, and they are being used in the treatment of malaria. In the medicinal chemistry literature, these structures are usually represented as in Scheme 4.

According to the above electronic-structure analysis, proguanil should be more appropriately represented, as in Scheme 5. Semi-empirical AM1 calculations on the conformational analysis of proguanil confirmed that the global minimum arrangement of proguanil shows an absence of hydrogen on N4, the chlorphenyl substitution should be on N6, and the isopropyl group should be on N3 of biguanide. Hence, the most suitable representation of the structure of pyrimethamine and proguanil are **32** and **33** (Scheme 5). (**32** is only a rotated representation of **31**.) Such a representation brings out the striking similarities between the two DHFR inhibitors and helps in realizing the pharmacophoric features. AM1 calculations have been performed on all the other biguanide derivatives given in Figure 1 to identify their global minimum conformations. The results indicate that in all the cases (i) a tautomer with H on N4 is less stable and (ii) the substituents prefer to be located on N6. Hence, the structures given in Figure 1 are not the true representation of the drugs/drug candidates; pertinent representations are given in Figure 7, and the 3D structures of the global minima on the respective potential energy surfaces are given in Figure 8. From this analysis, it is clear that in metformin the methyl substituent prefers to be on N3 or N7 but not on N1. In phenformin and other systems, the substituent prefers to occupy the N6 position. These differences may be leading to the observed differences in their antidiabetic activity. Further work is in progress to verify this hypothesis.

Conclusions

Electronic−structural studies on biguanide indicate that the global minimum tautomer is **10**. **10** is characterized by the following features: (i) C2−N4−C5−N6 4π-electron conjugation, (ii) N1−H8- - -N6 intramolecular hydrogen bond, (iii) low-energy barrier for the 1,5-H shift, (iv) greater stabilization due to protonation in comparison to guanidine, (v) greater probability of deprotonation to favor tautomerization in comparison to acetaldehyde, acetamide, and nitro methane, (vi) a very characteristic molecular electrostatic potential that does not effect protonation/deprotonation, etc. All of these characteristics are important in identifying the pharmacophoric features of biguanide. This electronic−structural analysis is useful in more appropriately representing the DHFR inhibitors pyrimethamine and proguanil. This study also indicated that the dynamism associated with the basic biguanide frame is quite high (due to tautomerism); this leads to the global minima with substituents at N6 rather than at other nitrogen centers. This study also helped in realizing the complementary electrostatic surface of the biomolecules for best interaction with biguanide derivatives, and hence, this electronic and structural study is expected to be useful in identifying the biological targets for biguanide derivatives.

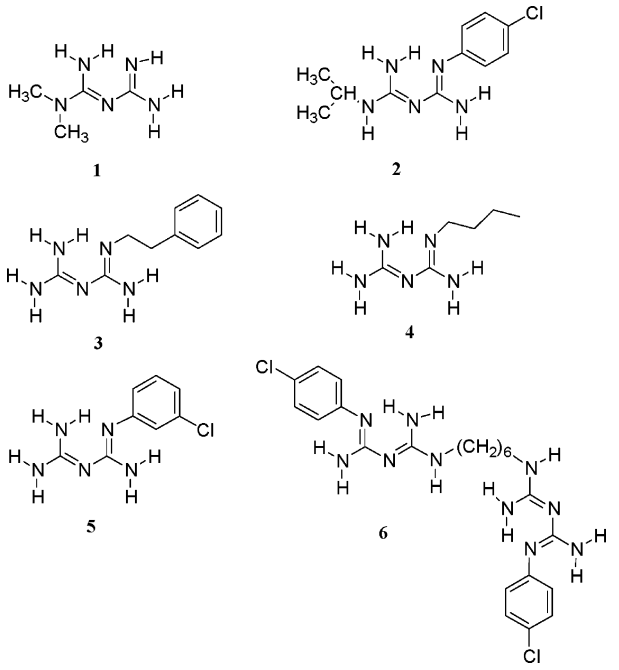

Figure 7. Correct conformers of important biguanide derivatives. These representations are different from those of Figure 1 in two counts (i) there is an absence of hydrogen on the N4 position, and (ii) the substituent groups occupy the N6 position, which leads to energy minimum conformations. The 3D representations of the same are given in Figure 8.

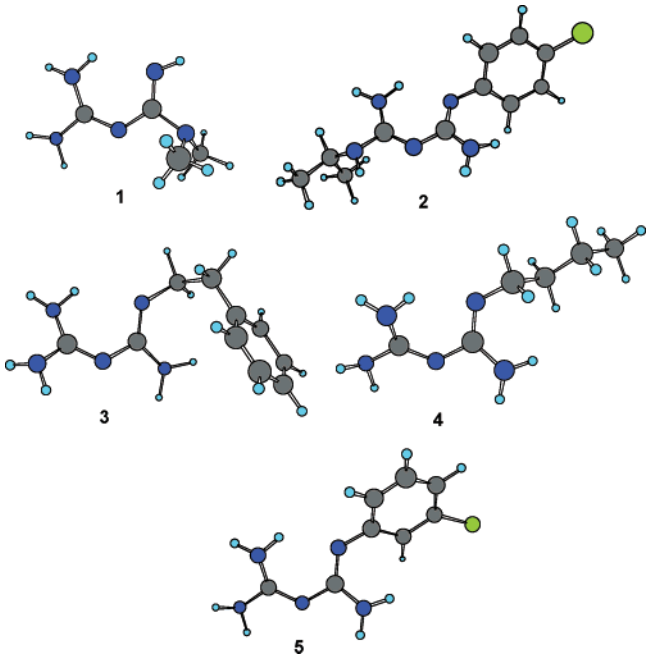

Figure 8. 3D structures of the most stable conformers of some important biguanide derivatives.

Acknowledgment. P.V.B. thanks the Department of Science and Technology (DST), New Delhi for financial support. P.I. thanks the Council of Scientific and Industrial Research (CSIR), New Delhi for financial

support under their New Millennium Initiatives (NMIT-LI) project.

Supporting Information Available: Tables S1−S6 with absolute energies of species under consideration, partial atomic charges, the second-order energies of various second-order interactions according to NBO analysis, and the HOMA analysis results. This material is available free of charge via the Internet at http://pubs.acs.org.

References

(1) Campbell, R. K.; White, J. R.; Saulie, B. A. Metformin: A New Oral Biguanide. *Clin. Ther.* **1996**, *18*, 360−371.

(2) Uchiyama, H.; Okamoto, A.; Sato, K.; Yamada, T.; Murakami, S.; Yoneda, S.; Kajita, Y.; Tegoshi, T.; Arrirono, N. Quinine-Resistant Severe Falciparum Malaria Effectively Treated with Atovaquone and Proguanil Hydrochloride Combination Therapy. *Intern. Med. (Tokyo, Jpn)* **2004**, *43*, 624−627.

(3) Davidoff, F.; Carr, S. Calcium-like Action of Phenethylbiguanide and Related Compounds: Inhibition of Pyruvate Kinase. *Proc. Natl. Acad. Sci. U.S.A.* **1972**, *69*, 1957−1961.

(4) Ohara, S.; Komatsu, R.; Matsuyama, T. Short-term Effect of Buformin, a Biguanide, on Insulin Sensitivity, Soluble Fraction of Tumor Necrosis Factor Receptor and Serum Lipids in Overweight Patient with Type 2 Diabetes Mellitus. *Diabetes Res. Clin. Pract*. **2004**, *66*, 133−138.

(5) Rahman, A. A.; Daoud, M. K.; Dukat, M.; Herrick-Davis, K.; Purohit, A.; Teitler, M.; Amaral, A. T.; Malvezzi, A.; Glennon, R. A. Conformationally-Restricted Analogues and Partition Coefficients of the 5-HT3 Serotonin Receptor Ligands *meta*-Chlorophenylbiguanide (mCPBG) and *meta*-Chlorophenylguanidine (mCPG). *Bioorg. Med. Chem*. **2003**, *13*, 1119−1123.

(6) Thomas, L.; Russell, A. D.; Maillard, J. Y. Antimicrobial Activity of Chlorhexidine Diacetate and Benzalkonium Chloride Against *Pseudomonas aeruginosa* and its Response to Biocide Residues. *J. Appl. Microbiol*. **2005**, *98*, 533−543.

(7) Denys, A.; Machlanski, T.; Bialek, J.; Mrozicki, S. Relation Between Chemical Structure and Antiviral Activity of Some Biguanide Derivatives. *Praeventivmedizin* **1977**, *164*, 85−89.

(8) Tanzer, J. M.; Slee, A. M.; Kamay, B. A. Structural Requirements of Guanide, Biguanide, and Bisbiguanide Agents for Antiplaque Activity. *Antimicrob. Agents Chemother*. **1977**, *12*, 721−729.

(9) Pinelli, A.; Trivulzio, S.; Pojaga, G.; Rossoni, G. Effects of 2-guanidine-4-methylquinazoline on Gastric Acid Secretion in Rats. *Pharmacol. Res*. **1996**, *34*, 225−230.

(10) Pinelli, A.; Colombo, R.; Trivulzio, S.; Berti, F.; Tofanetti, O.; Caimi, B. R. Inhibitory Effects of 2-Guanidinebenzimidazole and 1-Phenylbiguanide on Gastric Acid Secretion in Rats. *Arzneim.-Forsch.* **1984**, *34*, 890−894.

(11) Holland, W.; Morrison, T.; Chang, Y.; Wiernsperger, N.; Stith, B. J. Metformin (Glucophage) Inhibits Tyrosine Phosphatase Activity to Stimulate the Insulin Receptor Tyrosine Kinase. *Biochem. Pharmacol.* **2004**, *67*, 2081−2091.

(12) Zou, M. H.; Kirkpatrick, S. S.; Davis, B. J.; Nelson, J. S.; Wiles, W. G.; Schlattner, U.; Neumann, D.; Brownlee, M.; Freeman, M. B.; Goldman, M. H. Activation of the AMP-activated Protein Kinase by the Anti-diabetic Drug Metformin in vivo. *J. Biol. Chem.* **2004**, *279*, 43940−43951.

(13) Zhou, G.; Myers, R.; Li, Y.; Chen, Y.; Shen, X.; Fenyk-Melody, J.; Wu, M.; Ventre, J.; Doebber, T.; Fujii, N.; Musi, N.; Hirshman, M. F.; Goodyear, L. J.; Moller, D. E. Role of AMP-Activated Protein Kinase in Mechanism of Metformin Action. *J. Clin. Invest.* **2001**, *108*, 1167−1174.

(14) Hawley, S. A.; Gadalla, A. E.; Olsen, G. S.; Hardie, D. G. The Antidiabetic Drug Metformin Activates the AMP-Activated Protein Kinase Cascade via an Adenine Nucleotide-Independent Mechanism. *Diabetes* **2002**, *51*, 2420−2425.

(15) Sweeney, D.; Raymera, M. L.; Lockwood, T. D. Antidiabetic and Antimalarial Biguanide Drugs are Metal-Interactive Antiproteolytic Agents. *Biochem. Pharmacol.* **2003**, *66*, 663−677.

(16) Ruggiero-Lopez, D.; Lecomte, M.; Moinet, G.; Patereau, G.; Lagarde, M.; Wiernsperger, N. Reaction of Metformin with Dicarbonyl Compounds: Possible Implication in the Inhibition of Advanced Glycation End Product Formation. *Biochem. Pharmacol.* **1999**, *58*, 1765−1773.

(17) Mišur, I.; Turk, Z. Substituted Guanidine Compounds as Inhibitors of Nonenzymatic Glycation in vitro. *Croat. Chem. Acta* **2001**, *74*, 455−465.

(18) Glennon, R. A.; Daoud, M. K.; Dukat, M.; Teitler, M.; Herrick-Davis, K.; Purohit, A.; Syed, H. Arylguanidine and Arylbiguanide Binding at 5-HT3 Serotonin Receptors: A QSAR Study. *Bioorg. Med. Chem*. **2003**, *11*, 4449−4454.

(19) Setter, S. M.; Iltz, J. L.; Thams, J.; Campbell, R. K. Metformin Hydrochloride in the Treatment of Type 2 Diabetes Mellitus: A Clinical Review with a Focus on Dual Therapy. *Clin. Therap.* **2003**, *12*, 2991−3026.

(20) Pinkerton, A.; Schwarzenbach, D. Structural Studies on Biguanide and Related Species: Correlation of Protonation Energy with Molecular Structure. *J. Chem. Soc., Dalton Trans. B* **1978**, *34*, 989−996.

(21) Ray, P. Complex Compounds of Biguanides and Guanylureas with Metallic Elements. *Chem. Rev*. **1960**, 313−359.

(22) Das, G.; Bharadwaj, P. K.; Ghosh, D.; Chaudhuri, B.; Banerjee, R. Synthesis and Structure of the $[MnIV(biguanide)_3]_4^+$ ion: The Simplest Source for Water-Stable Manganese(IV). *Chem. Commun.* **2001**, 323−324.

(23) Anderson, K. B.; Franich, R. A.; Kroese, H. W.; Meder, R.; Rickard, C. E. F. The Structure of Biguanide Complexes of Boron. *Polyhedron* **1995**, *14*, 1149−1153.

(24) Marchi, A.; Marvelli, L.; Cattabriga, M.; Rossi, R.; Neves, M.; Bertolasi, V.; Ferretti, V. Technetium(V) and Rhenium(V) Complexes of Biguanide Derivatives: Crystal Structures. *J. Chem. Soc., Dalton Trans*. **1999**, 1937−1943.

(25) Coghi, L.; Lanfranchi, M.; Pelizzi, G.; Tarasconi, P. Structure Researches on the Chelating Behaviour of the Biguanide Ligand: The Crystal Structure of $Co(C_2H_6N_5)_3{\cdot}2H_2O$ and $Cu(C_2H_7N_5)_2CO_3{\cdot}4H_2O$. *Transition Met. Chem. (Dordrecht, Neth.)* **1978**, *3*, 69−76.

(26) Ernst, S. R.; Cagle, F. W., Jr. Biguanide. *Acta Crystallogr*., Sect. *B* **1977**, *33*, 235−237.

(27) Ernst, S. R. Biguanide Hydrochloride. *Acta Cryst*allogr., Sect. *B* **1977**, *33*, 237−240.

(28) Syamal, A. Crystal Data of Biguanide Dihydrochloride: $C_2H_7N_5{\cdot}$ 2HCl. *Indian J. Phys.* **1975**, *49*, 707−708.

(29) Gadre, S. R.; Shirsat, R. N. *Electrostatics of Atoms and Molecules*; Universities Press: Hyderabad, India, 2000.

(30) (a) Murray, J. S.; Politzer, P. The Use of Molecular Electrostatic Potential in Medicinal Chemistry. In *Quantum Medicinal Chemistry*. Wiley-VCH: New York, 2002; Vol. 17, pp 233−254. (b) Höltje, H.-D.; Höltje, M. Applications of Quantum Chemical Methods in Drug Design. *Quantum Medicinal Chemistry*; Wiley-VCH: New York, 2002; Vol. 17, pp 255−274.

(31) (a) Foresman, J. B.; Frisch, Æ. *Exploring Chemistry with Electronic Structure Methods;* Gaussian Inc.: Pittsburgh, PA, 1998. (b) Hehre, W. J.; Radom, L.; Schleyer, P. V. R.; Pople, J. A. *Ab Initio Molecular Orbital Theory*; Wiley: New York, 1985. (c) Ochterski, J. W. Thermochemistry in Gaussian. http://Gaussian.com/g_whitepap/thermo.htm.

(32) (a) Parr, R. G.; Yang, W. *Density Functional Theory of Atoms and Molecules*; Oxford University Press: New York, 1989. (b) Bartolotti, L. J.; Fluchick, K. In *Reviews in Computational Chemistry*; Lipkowitz, K. B., Boyd, D. B., Eds.; VCH Publishers: New York, 1996; Vol. 7, p 187.

(33) Frisch, M. J.; Trucks, G. W.; Schlegel, H. B.; Scuseria, G. E.; Robb, M. A.; Cheeseman, J. R.; Montgomery, J. A.; Vreven, T., Jr.; Kudin, K. N.; Burant, J. C.; Millam, J. M.; Iyengar, S. S.; Tomasi, J.; Barone, V.; Mennucci, B.; Cossi, M.; Scalmani, G.; Rega, N.; Petersson, G. A.; Nakatsuji, H.; Hada, M.; Ehara, M.; Toyota, K.; Fukuda, R.; Hasegawa, J.; Ishida, M.; Nakajima, T.; Honda, Y.; Kitao, O.; Nakai, H.; Klene, M.; Li, X.; Knox, J. E.; Hratchian, H. P.; Cross, J. B.; Adamo, C.; Jaramillo, J.; Gomperts, R.; Stratmann, R. E.; Yazyev, O.; Austin, A. J.; Cammi, R.; Pomelli, C.; Ochterski, J. W.; Ayala, P. Y.; Morokuma, K.; Voth, G. A.; Salvador, P.; Dannenberg, J. J.; Zakrzewski, V. G.; Dapprich, S.; Daniels, A. D.; Strain, M. C.; Farkas, O.; Malick, D. K.; Rabuck, A. D.; Raghavachari, K.; Foresman, J. B.; Ortiz, J. V.; Cui, Q.; Baboul, A. G.; Clifford, S.; Cioslowski, J.; Stefanov, B. B.; Liu, G.; Liashenko, A.; Piskorz, P.; Komaromi, I.; Martin, R. L.; Fox, D. J.; Keith, T.; Al-Laham, M. A.; Peng, C. Y.; Nanayakkara, A.; Challacombe, M.; Gill, P. M. W.; Johnson, B.; Chen, W.; Wong, M. W.; Gonzalez, C.; Pople, J. A. *Gaussian-03 suite of programs*; Gaussian, Inc.: Pittsburgh, PA, 2003.

(34) (a) Becke, A. D. Density-Functional Thermochemistry. III. The Role of Exact Exchange. *J. Chem. Phys.* **1993**, *98*, 5648−5652. (b) Lee, C.; Yang, W.; Parr, R. G. Development of the Colle-Salvetti Correlation-Energy Formula into a Functional of the Electron Density. *Phys. Rev. B* **1988**, *37*, 785−789. (c) Perdew, J. P.; Wang, Y. Accurate and Simple Analytic Representation of the Electron-Gas Correlation Energy. *Phys. Rev. B* **1992**, *45*, 13244−13249.

(35) Krishan, R.; Frisch, M. J.; Pople, J. A. Contribution of Triple Substitutions to the Electron Correlation Energy in Fourth Order Perturbation Theory. *J. Chem. Phys.* **1980**, *72*, 4244−4245.

(36) Scott, A. P.; Radom, L. Harmonic Vibrational Frequencies: An Evaluation of Hartree−Fock, Møller−Plesset, Quadratic Configuration Interaction, Density Functional Theory, and Semiempirical Scale Factors. *J. Phys. Chem.* **1996**, *100*, 16502−16513.

(37) Curtiss, L. A.; Raghavachari, K.; Pople, J. A. Gaussian-2 Theory Using Reduced Møller−Plesset Orders. *J. Chem. Phys.* **1993**, *98*, 1293−1298.

(38) (a) Reed, A. E.; Weinstock, R. B.; Wienhold, F. Natural Population Analysis. *J. Chem. Phys.* **1985**, *83*, 735−746. (b) Reed, A. E.; Wienhold, F.; Curtiss, L. A. Intermolecular Interactions from a Natural Bond Orbital, Donor−Acceptor Viewpoint. *Chem. Rev.* **1988**, *88*, 899−926.

(39) (a) Krygowski, T. M. Crystallographic Studies of Inter- and Intramolecular Interactions Reflected in Aromatic Character of Π.-Electron Systems. *J. Chem. Inf. Comput. Sci*. **1993**, *33*, 70−78. (b) Krygowski, T. M.; Cyrañski, M. K.; Anulewicz-Ostrowska, R. Guanidinium Cation−An Acyclic Analogue of Benzene? *Pol. J. Chem*. **2001**, *75*, 1939−1942.

(40) Hehre, W. J. *A Guide to Molecular Mechanics and Quantum Chemical Calculations*; Wavefunction: Irvine, 2001.

(41) An additional tautomeric form can be theoretically envisaged as shown below.

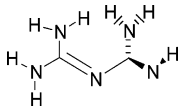

However, on the potential energy (PE) surface of biguanide, this tautomer could not be located. Complete optimization on this structure led to **10**.

(42) (a) Bharatam, P. V.; Iqbal, P.; Malde, A.; Tiwari, R. Electron Delocalization in Aminoguanidine: A Computational Study. *J. Phys. Chem.* **2004**, *108*, 10509−10517. (b) Lammertsma, K.; Prasad, B. V. Nitro ⇌ *aci*-Nitro Tautomerism. *J. Am. Chem. Soc.* **1993**, *115*, 2348−2351. (c) Lammertsma, K.; Prasad, B. V. Imine ⇌ Enamine Tautomerism. *J. Am. Chem. Soc.* **1994**, *116*, 642−650. (d) Lammertsma, K.; Bharatam, P. V. Keto ⇌ Enol, Imine ⇌ Enamine, Nitro ⇌ *aci*-Nitro Tautomerism and their Interrelationship in Substituted Nitroethylenes. Keto, Imine, Nitro, and Vinyl Substituent Effects and the Importance of H-bonding. *J. Org. Chem.* **2000**, *65*, 4662−4670.

(43) (a) Bharatam, P. V.; Moudgil, R.; Kaur, D. Electron Delocalization in Isocyanates, Formamides, and Ureas: Importance of Orbital Interactions. *J. Phys. Chem.* **2003**, *107*, 1627−1634. (b) Bharatam, P. V.; Uppal, P.; Amita, A. G.; Kaur, D. Theoretical Investigation on the Conformational Preferences in Sulfinimines. *J. Chem. Soc., Perkin Trans.* **2000**, *2*, 43. (c) Bharatam, P. V.; Amita, A. G.; Kaur, D. Electronic Structure of N-sulfenylimines. *J. Phys. Org. Chem.* **2003**, *16*, 183−189. (d) Moudgil, R.; Bharatam, P. V.; Kaur, R.; Kaur, D. Theoretical Studies on Electron Delocalization in Selenourea. *Proc. Ind. Acad. Sci. (Chem. Sci.)* **2002**, *114*, 223−230.

(44) Maksic, Z. B.; Kovacevic, B. Absolute Proton Affinity of Some Polyguanides. *J. Org. Chem*. **2000**, *65*, 3303−3309.

(45) Reaction used to calculate Gibbs free energy for protonation $G_{prot} = \Delta H_{298} - T\Delta S_{298}$ where ΔH_{298} is the enthalpy change and is calculated by the following equation: $\Delta H_{298} = [H_{298}(BH^+) - (H_{298}(B) + H_{298}(H^+))]$, T is the temperature (298.15 K), and ΔS_{298} is the entropy change and is calculated using the following equation: $\Delta S_{298} = [S_{298}(BH^+) - (S_{298}(B) + S_{298}(H^+))]$.

JM050602Z